OPEN

NPG Asia Materials (2016) 8, e293; doi:10.1038/am.2016.102
www.nature.com/am

ORIGINAL ARTICLE

Highly active nonprecious metal hydrogen evolution electrocatalyst: ultrafine molybdenum carbide nanoparticles embedded into a 3D nitrogen-implanted carbon matrix

Huabin Zhang[1,2], Zuju Ma[3], Guigao Liu[2], Li Shi[2], Jing Tang[2], Hong Pang[2], Kechen Wu[3], Toshiaki Takei[2], Jian Zhang[3], Yusuke Yamauchi[2] and Jinhua Ye[1,2]

The generation of clean and sustainable hydrogen fuel through water splitting demands efficient and robust earth-abundant catalysts for the hydrogen evolution reaction (HER). A new hybrid, which was fabricated by incorporating molybdenum carbide (Mo_xC) nanoparticles into a nitrogen-implanted three-dimensional carbon matrix (MoCN-3D), was developed as a highly active and durable nonprecious metal electrocatalyst for HER. The porous architecture of MoCN-3D can provide continuous mass transportation with a minimal diffusion resistance and thus produce effective electrocatalytic kinetics in both acidic and alkaline media. Experimental observations in combination with density functional theory calculations reveal that the effective coupling between molybdenum carbide nanoparticles and the carbon matrix, as well as N hybrid coordination, can modify the electronic Fermi level of the final hybrid, which synergistically reduces the proton adsorption and the reduction barrier during electrocatalytic HER.

NPG Asia Materials (2016) **8,** e293; doi:10.1038/am.2016.102; published online 22 July 2016

INTRODUCTION

Growing concerns about global warming and the depletion of petroleum resources have stimulated a great deal of interest in the development of novel technologies for clean and sustainable energy. The electrocatalytic reduction of water to molecular hydrogen via hydrogen evolution reaction (HER; $2H^+ + 2e \rightarrow H_2$) provides a promising solution to future energy supplies.[1–3] Platinum (Pt) remains the most efficient electrocatalyst for HER; however, the high cost and limited supply of Pt necessitate finding an alternative cheap and abundant catalyst for HER applications.[4] In recent years, a wide variety of transition metals (Co, Ni, Fe, Mo and W) and derivative components have been selected as effective candidates.[5–11] Particularly, β-phase molybdenum carbides have been demonstrated as highly active HER catalysts, even though they are bulky particles, and their performances could be further improved by constructing proper nanostructures.[12–17] It was revealed that nanorods of β-Mo_2C work better as an electrocatalyst for HER than bulk β-Mo_2C.[12] In addition to the morphology contribution, hybridization with heteroatom-doped graphitic carbon could further improve its performance because the effective coupling between β-Mo_2C and N-doped graphitic carbon can greatly modify the work function of the hybrid and thus reduce the proton adsorption and the reaction barrier.[16]

Other than tailoring the nanostructure and chemical composition of the catalysts, the HER behavior can also be optimized through the manipulation of the whole architecture of the electrocatalyst. Catalysts prepared in the form of one-dimensional or two-dimensional (2D) particles are randomly aggregated when preparing electrodes. The absence of pores in such electrodes leads to limited gas transport within them. Therefore, the precise control of active sites in an optimized framework is crucial to improve the performance of catalysts for HER. Particularly, ultrafine molybdenum carbide nanoparticles embedded in a nitrogen-implanted carbon matrix can work as a promising electrocatalyst because of their hierarchical pores, large surface area, high electrical conductivity and flexibility with the ability to provide continuous charge transportation with minimal diffusion resistance, thus enabling effective electrocatalytic kinetics.[18,19] However, the controllable synthesis of a composite constructed by nanostructured metal carbides coupled with a three-dimensional (3D) carbon matrix remains a great challenge because of the difficulty in achieving uniform carburization and the inevitable coalescence of nanoparticles at a high reaction temperature.

[1]TU-NIMS Joint Research Center, and Key Lab of Advanced Ceramics and Machining Techonology of Ministry of Education, School of Materials Science and Engineering, Tianjin University, Tianjin, PR China; [2]International Center for Materials Nanoarchitectonics (WPI-MANA), National Institute for Materials Science (NIMS), Ibaraki, Japan and [3]Fujian Institute of Research on the Structure of Matter, Chinese Academy of Sciences, Fujian, PR China
Correspondence: Professor J Ye, TU-NIMS Joint Research Center, and Key Lab of Advanced Ceramics and Machining Techonology of Ministry of Education, School of Materials Science and Engineering, Tianjin University, 92 Weijin Road, Nankai District, Tianjin 300072, PR China.
E-mail: yejinhua@tju.edu.cn or Jinhua.YE@nims.go.jp
Received 23 February 2016; revised 28 May 2016; accepted 30 May 2016

Very recently, metal–organic frameworks (MOFs), constructed using metal (clusters) and a carboxylate- and/or N-containing ligand from a huge array of choices, have been well developed as a class of ideal precursors.[20–25] Particularly, the zeolitic imidazolate frameworks (ZIFs) with a high carbon content and large surface area are a good candidate to synthesize porous carbon- and/or metal-based nanostructured composites, and the long-range ordering and high porosity of ZIFs can be partially preserved to afford homogeneously distributed heteroatoms in a carbon matrix with a high surface area.[23,24] However, MOF-derived materials are mainly limited to the Zn-, Cu-, Co- and Fe-based composites. Although Lou and colleagues developed an MOF-assisted strategy for synthesizing porous molybdenum carbide nanoparticles by introducing guest polyoxometalates into the pores of the MOF host, this is the only report indicating that a Mo-based hybrid can be constructed by the direct transformation of sole MOF precursor.[13]

In the current study, we constructed an unprecedented composite (MoCN-3D) derived from a recently developed hybrid zeolite imidazolate framework (HZIF), in which HZIF was organized by partly substituting the $Zn(im)_4^{2-}$ units in ZIF-8 with MoO_4^{2-} nodes.[25] MoCN-3D not only inherits the merits of carbon independently from ZIF, such as a large surface area and highly dispersed N-based active species, but also hybridizes zero-dimensional molybdenum carbide with a 3D graphitic carbon matrix to form a hierarchical heterostructured framework, which have rarely been achieved simultaneously in previous research.[13] Then, the composite was utilized as an HER electrocatalyst, which features the utmost exposure of active sites, a consecutive conductive network, and obvious synergistic effects between the components. Remarkably, the HZIF-derived hybrid exhibited excellent HER activity approaching the level of commercial Pt/C in both acid and alkaline media.

EXPERIMENTAL PROCEDURES

Synthesis of HZIF

$Zn(CH_3COO)_2{\cdot}2H_2O$ (0.2206 g, 1 mmol), 2-methylimidazole (2 mim, 0.1193 g, 1.5 mmol), molybdic acid (0.0401 g, 0.25 mmol), polyvinylpyrrolidone (300 mg) and *N*,*N*-dimethylformamide (12 ml) were combined in a 25 ml Teflon-lined airtight reactor that was heated at 160 °C for 48 h and then cooled to room temperature. The light green crystals were obtained as a pure phase, washed with water and ethanol, and dried at room temperature.

Preparation of MoCN-3D and MoCN-2D

For the preparation of MoCN-3D, HZIF powder was placed in a tube furnace under an Ar gas flow ($2\,l\,min^{-1}$), heated to 700 °C ($5\,°C\,min^{-1}$) and maintained at 700 °C for 2 h. In this process, the zinc component was reduced by carbon to generate evaporative Zn at such a high temperature, whereas the Mo component was reacted with carbon and produced nanosized molybdenum carbide particles. The system was naturally cooled to room temperature to obtain the final MoCN-3D nanocatalyst. To remove the unevaporated zinc component, the MoCN-3D samples were treated in a 0.5 M H_2SO_4 aqueous solution at 60 °C, which was followed by repeated filtrations and washings with deionized water.

A similar method to the one described above was used for the preparation of MoCN-2D, except that the precursor was not HZIF. The precursor of MoCN-2D was synthesized by mixing identical amounts of 2 mim (0.1193 g, 1.5 mmol), $Zn(CH_3COO)_2{\cdot}2H_2O$ (0.2206 g, 1 mmol) and molybdic acid (0.0401 g, 0.25 mmol) in a CH_3CH_2OH solution; CH_3CH_2OH was evaporated from the mixture, and a solid sample was collected.

Reaction conditions and activity evaluation

The electrochemical measurements were carried out using a three-electrode cell on a CH Instruments Model 650A electrochemical work station with various catalysts as the working electrode. A Pt wire was used as the counter electrode, whereas an Ag/AgCl electrode (in acid media) or a calomel electrode (in alkaline medium) was used as the reference electrode. Linear sweep voltammetry with a $5\,mV\,s^{-1}$ scan rate was carried out from 0 to −0.6 V (vs RHE) in an electrolyte solution under continuous purging with Ar. Before testing, the catalyst was cycled numerous times by cyclic voltammogram until a stable cyclic voltammogram curve was obtained. For the fabrication of the working electrode, 2.5 mg as-synthesized catalyst was mixed with a 30 µl Nafion solution (5.0% Nafion in ethanol) and 1000 µl deionized water. The mixture was sonicated. The suspension was pipetted out, dropped onto a glassy carbon electrode with a diameter of 3 mm and then fully dried. All the electrodes were prepared by depositing the same mass loading ($0.26\,mg\,cm^{-2}$) of active materials on a glassy carbon electrode using the same method. The product of H_2 was measured with a gas chromatograph (GC-8A, Shimadzu Co., Kyoto, Japan) with a thermal conductivity detector according to a standard curve. The Faradic efficiency of the HER catalysts is defined as the ratio of the amount of experimentally determined H_2 to that of the theoretically expected H_2 from the reaction. Electrochemical impedance spectra were tested at −0.4 V vs reversible hydrogen electrode (RHE) with frequencies from 0.1 to 1×10^5 Hz.

Characterization

X-ray diffraction patterns were recorded on an X-Pert diffractometer equipped with graphite monochromatized Cu-Kα radiation (PANalytical, Philips, Amsterdem, Netherlands). The specific surface areas were determined with a surface area analyzer (BEL Sorp-II mini, BEL Japan Co., Tokyo, Japan) by the Brunauer–Emmett–Teller method. Transmission electron microscopy (TEM) images were taken by a field-emission transmission electron microscope (2100F, JEOL Co., Tokyo, Japan) operated at 200 kV. An energy dispersive X-ray spectrometer (EDX) installed in the 2100F was used to analyze the microzone composition (scanning transition electron microscopy-energy dispersive X-ray spectrometer mapping). The scanning electron microscopy images were recorded on a field-emission scanning electron microscope (S4800, Hitachi Co., Tokyo, Japan) with an acceleration voltage of 10 kV. A surface chemical analysis was performed using X-ray photoelectron spectroscopy (XPS, PHI Quantera SXM, ULVAC-PHI Inc., Kanagawa, Japan). The evolved H_2 was analyzed using an online gas chromatograph (GC-8A, Shimadzu Co.) equipped with a thermal conductivity detector. Thermal gravimetric-differential thermal analysis (TG/DTA) was performed by using a DTG-60H instrument (Shimadzu Co.) from 25 to 700 °C under air at a heating rate of $10\,°C\,min^{-1}$.

Computation details

The generalized gradient approximation with the Perdew–Burke–Ernzerhof exchange-correlation function[16] (including long-range dispersion corrections developed by Grimme *et al.*) and a 450 eV cutoff for the plane-wave basis set were employed to perform all the density functional theory computations within the frame of the Vienna *ab initio* simulation package. The projector-augmented plane wave was used to describe the electron–ion interactions.[26] One gamma k-point was used in the simulations. All the structures were fully relaxed to the ground state, and the spin polarization was considered in all the calculations. The convergence of energy and forces were set to 10^{-5} eV and $0.05\,eV\,Å^{-1}$, respectively.

RESULTS

Embedding ultrafine molybdenum carbide nanoparticles into a 3D nitrogen-implanted carbon matrix

The partial substitution of $Zn(im)_4^{2-}$ units in ZIF-8 by MoO_4^{2-} nodes resulted in the assembly of HZIF with a general framework composition of $Zn_4(im)_6MoO_4$ (Scheme 1; Supplementary Figures S1–S3). Scanning electron microscope images further confirmed that the obtained HZIF consisted of uniformly dispersed crystals with a rhombic dodecahedral shape, which is similar to that of ZIF-8 (Figures 1a and b).[24,27] The precursor HZIFs underwent pyrolysis at a high temperature under an Ar atmosphere and resulted in a 3D carbon matrix-based composite. In this process, the zinc component was reduced by carbon to generate evaporative Zn at a high

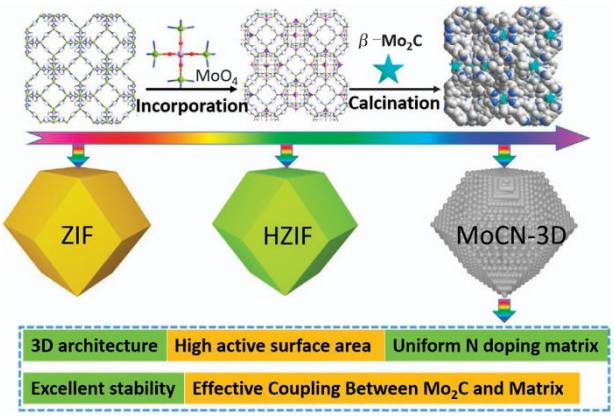

Scheme 1 Schematic illustration for the construction of MoCN-3D for a highly efficient hydrogen evolution reaction.

temperature, whereas the molybdenum component was converted to nanosized molybdenum carbide (Supplementary Figure S4).

As revealed by scanning electron microscopy images (Figure 1c), the obtained porous composite retained the original rhombic dodecahedron shape from the parent HZIF and exhibited a porous surface. A closer observation of the 3D carbon matrix further reveals a highly porous texture throughout the whole particle (Supplementary Figure S5). The porosity and more detailed structure of MoCN-3D were investigated by TEM and high-resolution TEM. The 3D carbon matrix was embedded with uniformly shaped nanoparticles with an average size of 4.0 nm without aggregation (Figures 1d–g; Supplementary Figure S6). The effective coupling between carbon layers and molybdenum carbide nanoparticles was also observed in the hybrid, as evidenced over the coating of the carbon layers over the nanoparticles (Figure 1g). Lattice fringes can be clearly observed in the high-resolution TEM images, in which the lattice spacing of 2.4 Å is

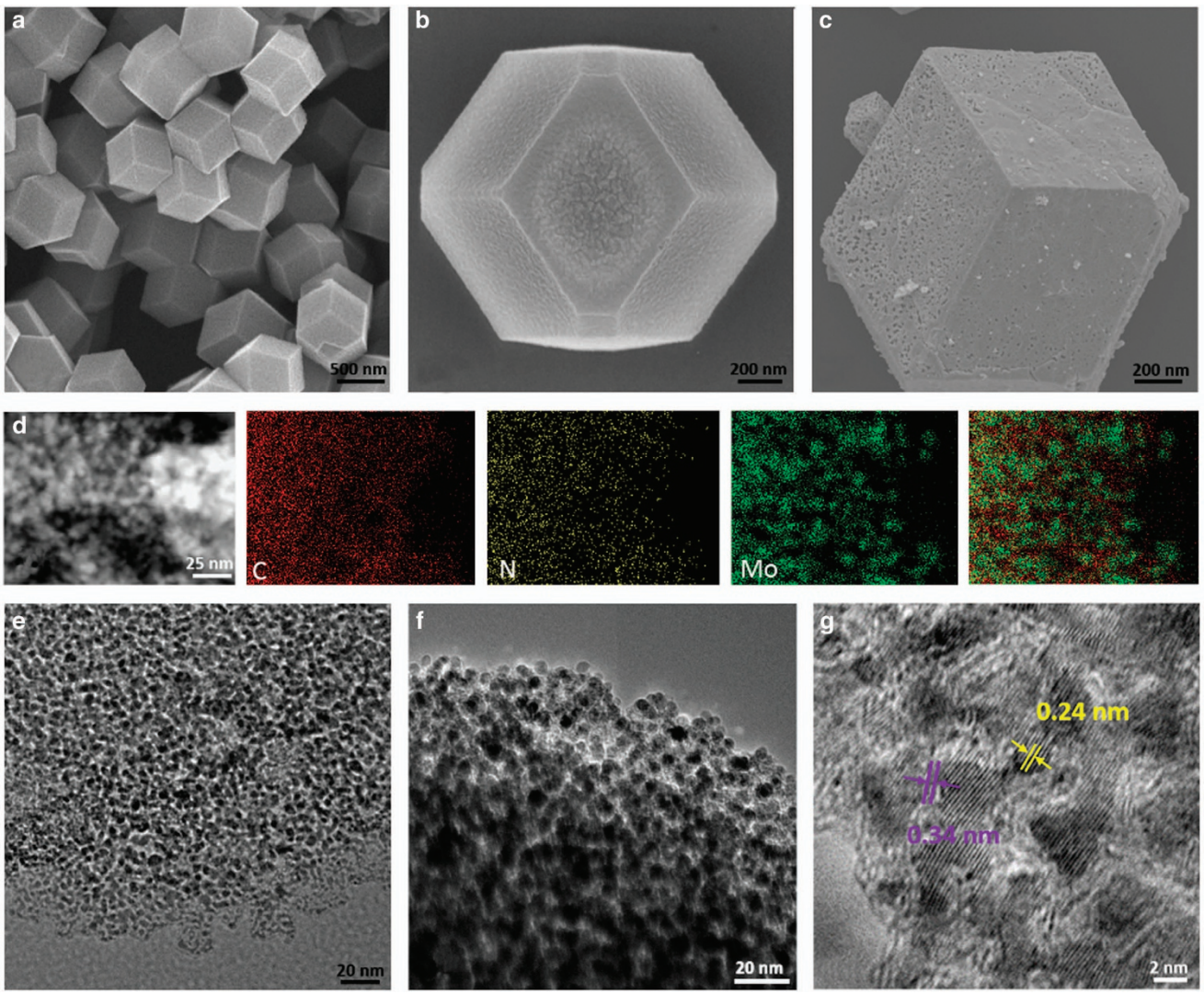

Figure 1 (**a**, **b**) Scanning electron microscopy images of HZIF-Mo crystals in different magnification and (**c**) HZIF-Mo-derived hybrid MoCN-3D. (**d**) Scanning transition electron microscopy image, C, N, Mo and combined element mapping images of HZIF-Mo-derived compound MoCN-3D. (**e**, **f**) TEM images of compound MoCN-3D. (**e**, **f**) High-resolution TEM images of the hybrid, showing the effective coupling between the carbon layers and molybdenum carbide nanoparticles. Insets are the (002) interplane space of molybdenum carbide and (002) plane of graphene (**g**).

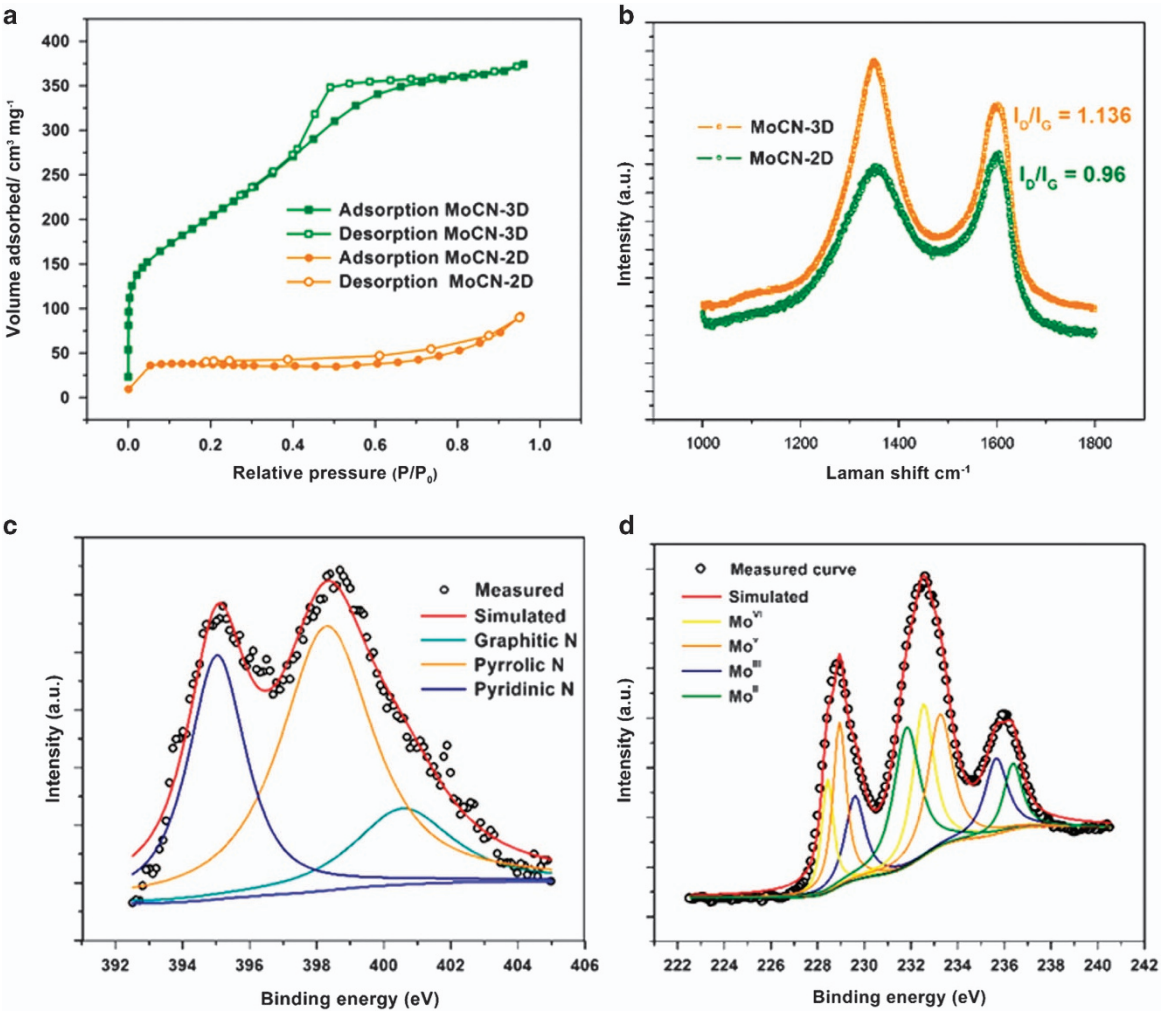

Figure 2 (**a**) N_2 adsorption – desorption isotherms for MoCN-3D and MoCN-2D. (**b**) Raman spectrum of MoCN-3D and MoCN-2D; the intensity ratio between D and G bands (I_D/I_G) was also calculated. (**c**) N 1*s* core level XPS spectrum. The high-resolution XPS spectra for N 1*s* in MoCN-3D exhibit three types of nitrogen species: dominant graphitic-N, pyridinic-N, as well as pyrrolic-N. (**d**) XPS Mo 3*d* spectrum and the sum of the peak-fitted curves.

assigned to the (0 0 2) interplane spacing of the molybdenum carbide nanoparticles, and the 3.4 Å belongs to the (0 0 2) plane of graphene (Figure 1g), revealing that graphitic carbons were formed by catalytic graphitization of amorphous carbon on the deposited Mo component.[14,16] The X-ray diffraction spectrum clearly reveals the formation of β-Mo_2C in MoCN-3D with a trace of MoC (Supplementary Figure S7). Scanning transition electron microscopy further confirmed the presence of numerous small nanoparticles homogenously distributed. The nature of the doping of the hybrid and the distribution of nanoparticles was revealed by the elemental mapping images of C, N and Mo (Figure 1d; Supplementary Figure S11). As expected, N atoms and Mo_2C are homogeneously distributed over the carbon sheets. A reference compound containing molybdenum carbide particles and N-doped carbon (denoted as MoCN-2D) was also constructed with the same annealing strategy but from a different precursor. X-ray diffraction and TEM investigations not only confirmed the formation of molybdenum carbide but also reveal that the molybdenum carbide nanoparticles are not distributed evenly in MoCN-2D, which is attributed to the uneven distribution of the Mo content in the precursor (Supplementary Figures S8 and S9).

The porosity of MoCN-3D was investigated by N_2 adsorption and desorption isotherms. The type IV isotherm and the pore size distribution curve confirmed the interconnected hierarchically micro/mesoporous structure in MoCN-3D, which might originate from the porous HZIF and the evaporation of Zn during the heat treatment (Figure 2a; Supplementary Figure S10).[28] The specific surface area of MoCN-3D was confirmed to be 706.3 $m^2 g^{-1}$, and this value is much higher than previously reported molybdenum carbide-based hybrid; as well as reference compound, MoCN-2D (41.7 $m^2 g^{-1}$).[13–16] The high porosity of MoCN-3D not only offers sufficient active sites but also favors electrolyte penetration and ion diffusion to facilitate the HER process, which is expected to produce a superior hydrogen evolution performance (Supplementary Figure S14). The graphitization degree of the carbon phase in different samples is characterized by Raman spectroscopy (Figure 2b). The characteristic D band and G band are observed at ~1355 and 1585 cm^{-1}, respectively. The presence of sp^2 carbon indicated by the G band is probably due to the catalytic graphitization of carbon by the Mo component. The intensity ratio of the D band to the G band (I_D/I_G) was confirmed to be 1.136 for MoCN-3D and 0.96 for MoCN-2D, which indicates that the structural disorder of the carbon support is more apparent in MoCN-3D.[27] XPS further reveals that a

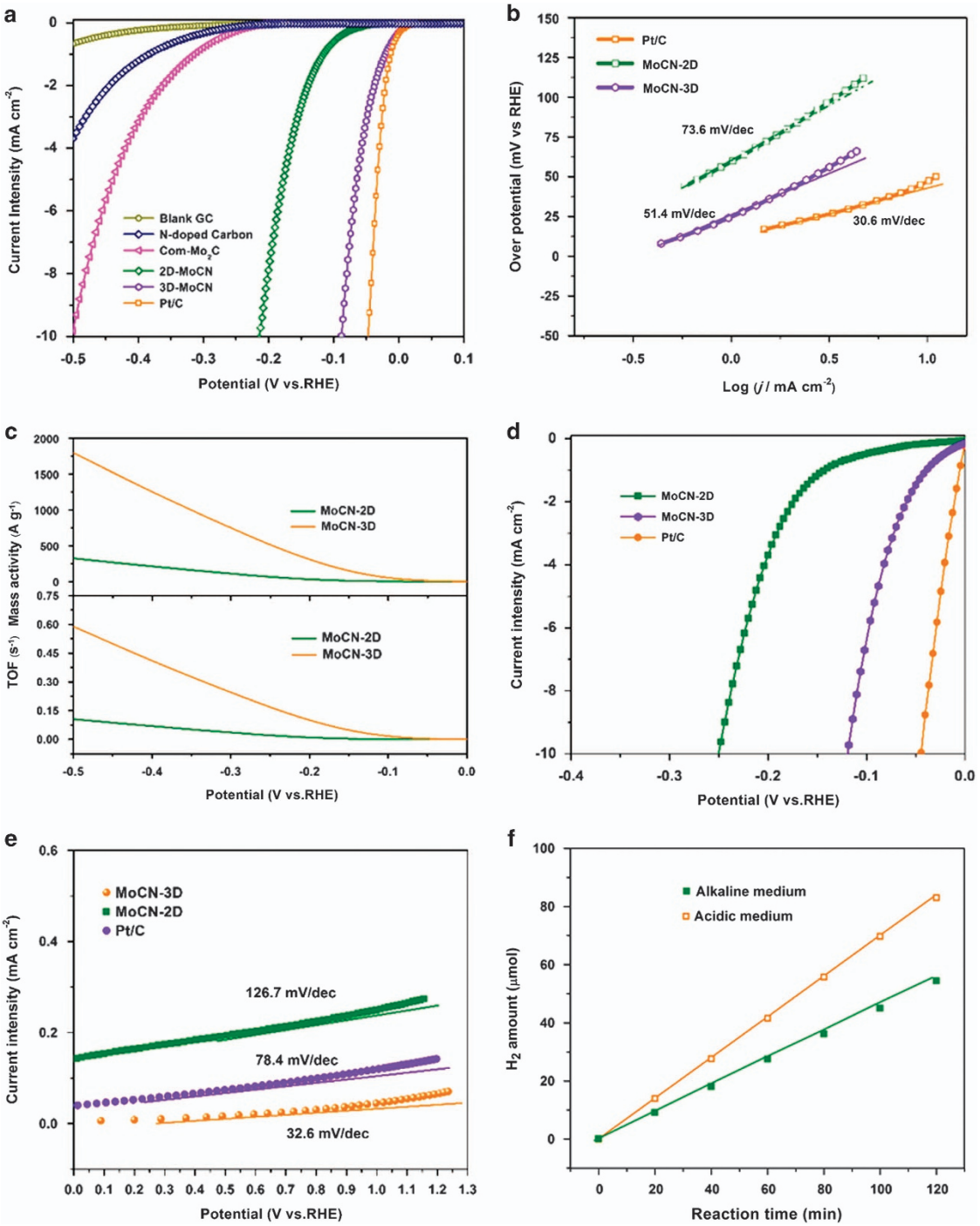

Figure 3 (**a**) The HER polarization curves of various catalysts in 0.5 M H_2SO_4, and (**b**) corresponding Tafel plots for various catalysts. (**c**) Mass activities (top) and TOF values (bottom) of catalysts at different overpotentials. (**d**) The HER polarization curves of various catalysts in 1 M KOH and (**e**) corresponding Tafel plots for various catalysts. (**f**) The amount of theoretically calculated (solid line) and experimentally measured (squares) hydrogen versus time for MoCN-3D at –0.2 V for 120 min.

significant amount of N is incorporated in MoCN-3D. The high-resolution XPS spectrum for N 1*s* in MoCN-3D exhibits three types of nitrogen species: the dominant graphitic-N, pyridinic-N and pyrrolic-N. All these N atoms can have an important influence on the final HER catalytic performance (Figure 2c).[23,24] The Mo 3*d* core level XPS spectrum is split into $3d_{5/2}$ and $3d_{3/2}$ peaks because of spin–orbital coupling. The peak fitting for the Mo 3*d* XPS peak of MoCN-3D confirms that there are four oxidation states (+2, +3, +4 and +6) for Mo on the surface of the molybdenum carbide nanoparticles. The existence of a Mo component in high valence states is attributed to the surface oxidation of the molybdenum carbide in air (Figure 2d).[29]

Catalytic performance

The HER performances of the as-prepared hybrids are evaluated as electrocatalysts in both acidic and basic aqueous solutions. The

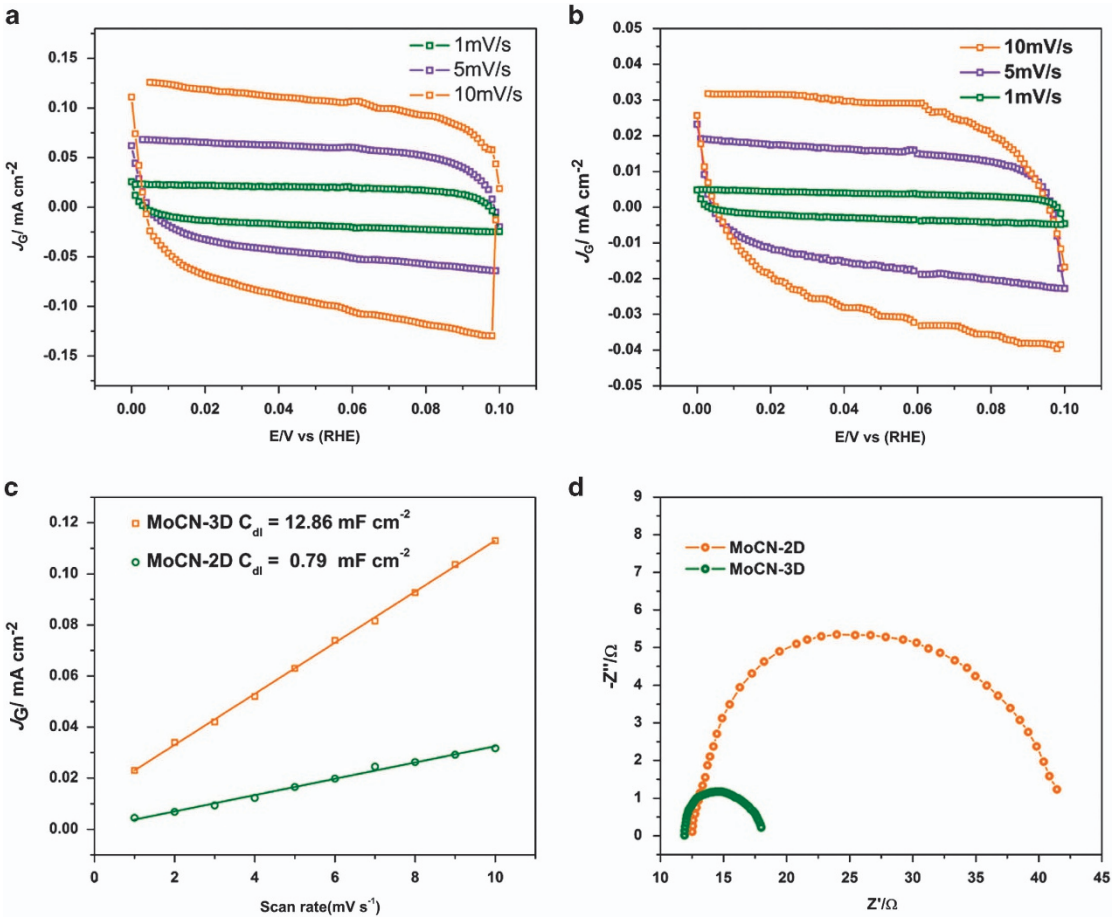

Figure 4 Cyclic voltammograms of MoCN-3D (**a**) and MoCN-2D (**b**) are taken in a potential window without faradaic processes. The capacitive currents as a function of scan rate for MoCN-3D and MoCN-2D (**c**), and electrochemical impedance spectra at −0.4 V vs RHE of MoCN-3D and MoCN-2D (**d**).

electrocatalytic activities of the composites were firstly evaluated in an Ar-saturated 0.5 M H_2SO_4 medium. As a reference, a commercial Pt catalyst (20 wt % Pt/C), N-doped carbon and commercially available Mo_2C (com-Mo_2C) were also measured at the same loading weight. As shown in Figure 3a, the blank glassy carbon electrode and N-doped carbon showed negligible or poor HER activities, whereas com-Mo_2C produced a current density of 1 mA cm^{-2} at an overpotential (η) of 335 mV. In contrast, the hybrid catalysts, MoCN-2D and MoCN-3D, exhibited apparent electrocatalytic activities for HER that were much higher than those of com-Mo_2C and N-doped carbon, which clearly indicated that the coupling between the carbon layers and molybdenum carbide can effectively influence the catalytic performance. It should be noted that the polarization curves show that MoCN-3D produces the best catalytic performance and exhibits a small overpotential of 89 mV (all the potentials are referenced to RHE in current study) to achieve a current density (J) of 10 mA cm^{-2}, which is very close to that of commercial Pt/C (Figure 3a). This value is notably more positive than that of MoCN-2D (approximately −218 mV), clearly suggesting that the advanced architecture in MoCN-3D is highly advantageous for effective HER. This fact can also be confirmed by a turnover frequency (TOF) and mass activity investigation. The TOFs for MoCN-3D were calculated to be 0.017 s^{-1} at $\eta = 100$ mV and 0.245 s^{-1} at $\eta = 300$ mV, which are much higher than those (0.001 at $\eta = 100$ mV and 0.035 at $\eta = 300$ mV) for MoCN-2D under identical conditions (Figure 3c). As each individual molybdenum atom was treated as a potential active site for the reaction, these calculations represent the best figure of merit for comparing activities among different catalysts.

To investigate the kinetics of the HER processes promoted by the as-prepared catalysts, a further analysis of the HER performance was carried out by analyzing Tafel plots at low overpotentials (Figure 3b). MoCN-3D gave a Tafel slope of 51.4 mV dec^{-1}, which is lower than that of MoCN-2D (73.6 mV dec^{-1}), revealing the higher HER rate and favorable kinetics of MoCN-3D. The Tafel slope value of 51.4 mV dec^{-1} also indicates that the electrochemical desorption Heyrovsky step is the rate determining step; therefore, a Volmer–Heyrovsky mechanism can be determined for the HER process catalyzed by MoCN-3D.[30,31] The exchange current density (j_0), as one of the most important parameters to illustrate catalytic efficiency, can be calculated by extrapolating the Tafel plots to the J axis. As expected, the obtained j_0 of MoCN-3D is 0.047 mA cm^{-2}, higher than that of MoCN-2D (0.012 mA cm^{-2}) and it is also one of the largest values among reported results.[5,6] The higher j_0 of MoCN-3D suggests a better catalytic efficiency, further confirming the favorable HER kinetics at the interface between MoCN-3D and the electrolyte. Combined with the polarization curves analyzed above, we may safely draw the conclusion that the 3D porous structure not only contributes to the charge transfer but can also produce an enlarged active area and thus contribute favorably to the final hydrogen evolution. These results also reveal that MoCN-3D is among the most active nonprecious HER electrocatalysts in acidic solutions [6–20,32–38] (Supplementary Tables S3 and S4).

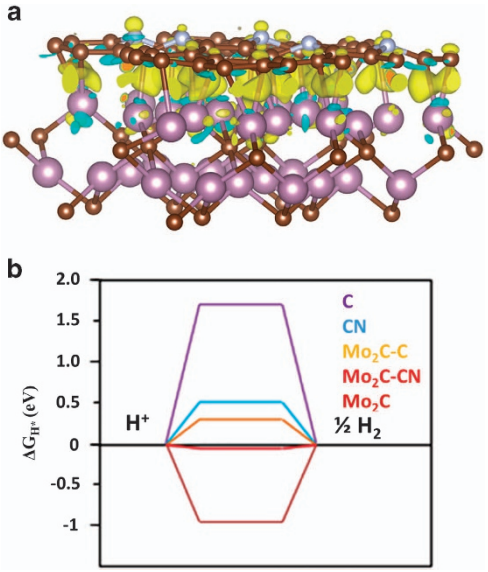

Figure 5 (**a**) Three-dimensional charge density difference for Mo_2C-CN composite with an isovalue of 0.0006 e A^{-3}. Yellow and blue isosurfaces represent charge accumulation and depletion in the space with respect to isolated Mo_2C and C layer. (**b**) Gibbs free energy (ΔG) profile of the HER on various catalysts.

The electrocatalytic activities of the catalysts for HER in an Ar-saturated basic medium were also investigated (1 M KOH). As shown in Figure 3d, MoCN-3D also exhibited good electrocatalytic activity for HER. The polarization curve of MoCN-3D showed that a small overpotential of 122 mV (vs RHE) can lead to a current density (J) of 10 mA cm^{-2}. This value compares favorably with those reported for most of the nonprecious metal HER catalysts under similar conditions and also outperforms MoCN-2D (249 mV).[9–11] The MoCN-3D catalyst shows a Tafel slope of 78.4 mV dec^{-1} in the basic solution, which is lower than that of MoCN-2D (126.7 mV dec^{-1}) (Figure 3e). These values compare favorably with the values reported for most nonprecious metal HER catalysts under similar conditions, such as cobalt-based catalysts,[31] tungsten sulfide[5] and iron-doped molybdenum carbide.[14] These results further confirmed that the incorporation of molybdenum carbide nanoparticles into the nitrogen-implanted three-dimensional carbon matrix (MoCN-3D) can effectively produce excellent performance in both acidic and alkaline media.

The durability of MoCN-3D as the HER catalyst electrode in acidic and alkaline media was investigated by electrolysis at fixed potentials over extended periods of time, as displayed in the current (i)–time (t) curve (Supplementary Figures S12a and S13a). MoCN-3D demonstrates an excellent stability with $<5\%$ degradation of the initial current after operating for 10 h in both acidic and alkaline media. The fluctuation displayed in the i–t curve can be attributed to the hydrogen gas generation, accumulation and desorption during the HER process. In addition, long-term potential cycling was performed using polarization curves at an accelerated scanning rate. There was only a slight decrease observed in the HER activity after 2000 cycles in acidic and alkaline media, further displaying the excellent durability (Supplementary Figures S12b and S13b). The surface compositions of the MoCN-3D catalyst recycled after the electrical catalytic reaction were further characterized by XPS (Supplementary Figure S15). There were no obvious changes in the spectra obtained before and after the reaction, which clearly confirms the maintenance of the original framework of MoCN-3D. Furthermore, TEM was performed after the reaction, and the representative high-resolution TEM images of the surface regions of MoCN-3D before and after the electrical catalytic reaction are shown in Supplementary Figure S16. After the reaction, most of the molybdenum carbide nanoparticles still maintain their original morphology, which further confirms the high stability of MoCN-3D. The excellent performance in high activity, favorable kinetics and strong durability reveal that MoCN-3D is a promising HER electrocatalyst.

The product of H_2 was confirmed by gas chromatography (GC) analysis and measured quantitatively using a thermal conductivity detector according to a standard curve. The potentiostatic cathodic electrolysis was operated by maintaining a MoCN-3D-loaded glassy carbon plate at an overpotential of 200 mV for 120 min both in 0.5 M H_2SO_4 and 1 M KOH solutions. The Faradic efficiency was calculated by comparing the amount of measured hydrogen with the amount of calculated hydrogen (Figure 3f).[36] Virtually, a 100% Faradic efficiency was obtained under both acidic and alkaline conditions, suggesting the current density is directly related to the hydrogen generation.

DISCUSSION

As confirmed from these results, we may find that the architecture of the catalyst has a vital role in the HER catalysis. To further understand the origin of the differences in the overall catalytic performance between MoCN-2D and MoCN-3D, we investigated their relative electrochemically active surface areas (ECSAs) by extracting the double-layer capacitance (C_{dl}) from the cyclic voltammetry measurements, which is believed to be positively proportional to the ECSA.[39] As observed, the C_{dl} of MoCN-3D (12.86 mF cm^{-2}) is substantially larger than that of MoCN-2D (0.79 mF cm^{-2}; Figures 4a–c). This should provide direct evidence for the enlarged ECSA of MoCN-3D. The enlarged ECSA not only provides additional active sites but also facilitates the fast transport of reactants and products for favorable HER kinetics. Moreover, the favorable kinetics were also verified using electrochemical impedance spectroscopy at -0.4 V (Figure 4d). The charge transfer resistance (R_{ct}) obtained from the semicircle in the low-frequency zone is related to the electrocatalytic kinetics at the interface between the catalyst and the electrolyte, and a lower value reveals a faster electron transfer. The MoCN-3D hybrid has an R_{ct} of $\sim 18\ \Omega\ cm^2$, which is much smaller than that of MoCN-2D ($44\ \Omega\ cm^2$), suggesting a more efficient electron transfer resulting in more favorable HER kinetics for the MoCN-3D catalyst.[40]

Density functional theory calculations were performed to investigate the electronic structure and H* adsorption-free energy of the hybrid structure. A good catalyst should feature a moderate free energy for H adsorption $|\Delta G_{H^*}|$ (close to zero) to compromise the reaction barriers in the adsorption and desorption processes.[16] Our calculations of the $|\Delta G_{H^*}|$ values for the surfaces of various catalysts are described in Figure 5 and Supplementary Table S2. The free energy for H* adsorption on the Mo_2C cluster was revealed to be rather strong, whereas it was rather weak on the carbon; this results in low HER activities in both cases. The static energy calculations show that, upon effective coupling between the carbon layers and the Mo_2C nanoparticles, the ΔG_{H^*} of carbon atoms bonded with Mo_2C decreases from 1.78 to 0.28 eV, resulting in a more favorable H* adsorption – desorption property (Supplementary Figure S17). In particular, the synergistic effects between the Mo_2C nanoparticles and the N dopants in Mo_2C-NC were obtained by the change in its valence orbital energy levels and resulting in the smallest $|\Delta G_{H^*}|$ value

of 0.006 eV. Our study shows that the effective coupling between a carbon sheet and a Mo_2C nanocluster can significantly modify the electronic Fermi level of the carbon sheet through charge transfer from Mo_2C to the nearby carbon atoms; moreover, it can be further activated by N doping. When Mo_2C and N are simultaneously introduced to form dual-modified Mo_2C-CN composites, the 2*p* orbital of the C is firstly polarized by Mo_2C, which is then able to donate extra electrons to an adjacent N atom. Consequently, not only the electron-donating Mo_2C but also the electron-accepting C and N atoms are activated as the asymmetrical spin and charge density are introduced. The above analysis clearly revealed that the effective coupling between the carbon layers and the Mo_2C nanoparticles, as well as the incorporation of N into the carbon matrix, produce a synergistic effect in tuning the ΔG_{H^*} to near zero and hence is responsible for the outstanding HER catalysis.

In summary, we constructed bimetallic MOFs as templates/precursors to afford a porous molybdenum carbide framework with a high surface area, a high degree of graphitization and a uniform N dopant profile by pyrolysis. Furthermore, we first achieved the direct transformation of MOF to a molybdenum carbide and nitrogen-implanted carbon matrix composite. The HER evaluation revealed that the catalysts showed excellent activities with large current densities, small Tafel slopes and outstanding electrochemical durability in both acidic and alkaline media. The excellent HER performances can be attributed to the 3D hierarchical porous structure, the high coupling between the active Mo_2C nanoparticles and the carbon layers, and the introduction of additional active sites resulting from the homogenous nitrogen doping of the graphitized carbon sheets. The hierarchical architecture of MoCN-3D can be used as a catalyst electrode that has the potential to replace Pt as a commercial HER catalyst. Furthermore, this novel strategy for the construction of low-cost catalysts using MOF templates might be extended to other similar systems to help pave the way towards the development of advanced electrodes replacing Pt/C in energy storage and conversion.

CONFLICT OF INTEREST

The authors declare no conflict of interest.

ACKNOWLEDGEMENTS

This work was partly supported by the National Basic Research Program of China (973 Program, 2014CB239301) and the World Premier International Research Center Initiative (WPI Initiative) on Materials Nanoarchitectonics (MANA), MEXT, Japan, and the Mitsubishi Foundation.

1 Thomas, J. G. N. Kinetics of electrolytic hydrogen evolution and the adsorption of hydrogen by metals. *Trans. Faraday Soc.* **57**, 1603–1611 (1961).
2 Turner, J. A. Sustainable hydrogen production. *Science* **305**, 972–974 (2004).
3 Zou, X. & Zhang, Y. Noble metal-free hydrogen evolution catalysts for water splitting. *Chem. Soc. Rev.* **44**, 5148–5180 (2015).
4 Stamenkovic, V. R., Mun, B. S., Arenz, M., Mayrhofer, K. J. J., Lucas, C. A., Wang, G., Ross, P. N. & Markovic, N. M. Trends in electrocatalysis on extended and nanoscale Pt-bimetallic alloy surfaces. *Nat. Mater.* **6**, 241–247 (2007).
5 Duan, J., Chen, S., Chambers, B. A., Andersson, G. G. & Qiao, S. Z. 3D WS_2 nanolayers@heteroatom-doped graphene films as hydrogen evolution catalyst electrodes. *Adv. Mater.* **27**, 4234–4241 (2015).
6 Acevedo, M. C., Stone, M. L., Schmidt, J. R., Thomas, J. G., Ding, Q., Chang, H.-C., Tsai, M. L., He, J. H. & Jin, S. Efficient hydrogen evolution catalysis using ternary pyrite-type cobalt phosphosulphide. *Nat. Mater.* **14**, 1245–1251 (2015).
7 Du, N., Wang, C., Wang, X., Lin, Y., Jiang, J. & Xiong, Y. Trimetallic TriStar nanostructures: tuning electronic and surface structures for enhanced electrocatalytic hydrogen evolution. *Adv. Mater.* **28**, 2077–2084 (2016).
8 Tian, J., Liu, Q., Cheng, N., Asiri, A. M. & Sun, X. Self-supported Cu3P nanowire arrays as an integrated high-performance three-dimensional cathode for generating hydrogen from water. *Angew. Chem. Int. Ed.* **53**, 9577–9581 (2014).
9 Laursen, A. B., Patraju, K. R., Whitaker, M. J., Retuerto, M., Sarkar, T., Yao, N., Ramanujachary, K. V., Greenblatt, M., Dismukes, G. C. Nanocrystalline Ni_5P_4: a hydrogen evolution electrocatalyst of exceptional efficiency in both alkaline and acidic media. *Energy Environ. Sci.* **8**, 1027–1034 (2015).
10 Miao, J., Xiao, F.-X., Yang, H. B., Khoo, S. Y., Chen, J., Fan, Z., Hsu, Y. Y., Chen, H. M., Zhang, H. & Liu, B. Hierarchical Ni-Mo-S nanosheets on carbon fiber cloth: A flexible electrode for efficient hydrogen generation in neutral electrolyte. *Sci. Adv.* **1**, e1500259 (2015).
11 Feng, L.-L., Yu, G., Wu, Y., Li, G., Li, H., Sun, Y., Asefa, T., Chen, W. & Zou, X. High-index faceted Ni_3S_2 nanosheet arrays as highly active and ultrastable electrocatalysts for water splitting. *J. Am. Chem. Soc.* **137**, 14023–14026 (2015).
12 Ma, F.-X., Wu, H. B., Xia, B. Y., Xu, C.-Y. & Lou, X. W. D. Hierarchical β-Mo_2C nanotubes organized by ultrathin nanosheets as a highly efficient electrocatalyst for hydrogen production. *Angew. Chem. Int. Ed.* **54**, 15395–15399 (2015).
13 Wu, H. B., Xia, B. Y., Yu, L., Yu, X. Y. & Lou, X. W. Porous molybdenum carbide nano-octahedrons synthesized via confined carburization in metal-organic frameworks for efficient hydrogenproduction. *Nat. Commun.* **6**, 6512 (2015).
14 Wan, C. & Leonard, B. M. Iron-doped molybdenum carbide catalyst with high activity and stability for the hydrogen evolution reaction. *Chem. Mater.* **27**, 4281–4288 (2015).
15 Liao, L., Wang, S., Xiao, J., Bian, X., Zhang, Y., Scanlon, M. D., Hu, X., Tang, Y., Liu, B., Girault, H. H. A nanoporous molybdenum carbide nanowire as an electrocatalyst for hydrogen evolution reaction. *Energy Environ. Sci.* **7**, 387–392 (2014).
16 Liu, Y., Yu, G., Li, G.-D., Sun, Y., Asefa, T., Chen, W. & Zou, X. Coupling Mo_2C with nitrogen-rich nanocarbon leads to efficient hydrogen-evolution electrocatalytic sites. *Angew. Chem. Int. Ed.* **54**, 10752–10757 (2015).
17 Fan, M., Chen, H., Wu, Y., Feng, L.-L., Liu, Y., Li, G.-D., Zou, X. Growth of molybdenum carbide micro-islands on carbon cloth toward binder-free cathodes for efficient hydrogen evolution reaction. *J. Mater. Chem. A* **3**, 16320–16326 (2015).
18 Wang, Z.-L., Hao, X.-F., Jiang, Z., Sun, X.-P., Xu, D., Wang, J., Zhong, H. X., Meng, F. L. & Zhang, X. B. C and N hybrid coordination derived Co–C–N complex as a highly efficient electrocatalyst for hydrogen evolution reaction. *J. Am. Chem. Soc.* **137**, 15070–15073 (2015).
19 Kibsgaard, J., Chen, Z., Reinecke, B. N. & Jaramillo, T. F. Engineering the surface structure of MoS_2 to preferentially expose active edge sites for electrocatalysis. *Nat. Mater.* **11**, 963–969 (2012).
20 Long, J. R. & Yaghi, O. M. The pervasive chemistry of metal–organic frameworks. *Chem. Soc. Rev.* **38**, 1213–1214 (2009).
21 Zhou, H.-C., Long, J. R. & Yaghi, O. M. Introduction to metal–organic frameworks. *Chem. Rev.* **112**, 673–674 (2012).
22 Zhang, H., Liu, G., Shi, L., Liu, H., Wang, T. & Ye, J. Engineering coordination polymers for photocatalysis. *Nano Energy* **22**, 149–168 (2016).
23 Chen, Y.-Z., Wang, C., Wu, Z.-Y., Xiong, Y., Xu, Q., Yu, S.-H. & Jiang, H. L. From bimetallic metal-organic framework to porous carbon: high surface area and multicomponent active dopants for excellent electrocatalysis. *Adv. Mater.* **27**, 5010–5016 (2015).
24 Tang, J., Salunkhe, R. R., Liu, J., Torad, N. L., Imura, M., Furukawa, S. & Yamauchi, Y. Thermal conversion of core–shell metal–organic frameworks: a new method for selectively functionalized nanoporous hybrid carbon. *J. Am. Chem. Soc.* **137**, 1572–1580 (2015).
25 Wang, F., Liu, Z.-S., Yang, H., Tan, Y.-X. & Zhang, J. Hybrid zeolitic imidazolate frameworks with catalytically active TO_4 building blocks. *Angew. Chem. Int. Ed.* **50**, 450–453 (2011).
26 Norskov, J. K., Bligaard, T., Logadottir, A., Kitchin, J. R., Chen, J. G., Pandelov, S., Stimming, U. Trends in the exchange current for hydrogen evolution. *J. Electrochem. Soc.* **152**, J23–J26 (2005).
27 Zhang, H., Ma, Z., Duan, J., Liu, H., Liu, G., Wang, T., Chang, K., Li, M., Shi, L., Meng, X., Wu, K. & Ye, J. Active sites implanted carbon cages in core–shell architecture: highly active and durable electrocatalyst for hydrogen evolution reaction. *ACS Nano.* **10**, 684–694 (2016).
28 Liang, J., Jiao, Y., Jaroniec, M. & Qiao, S. Z. Sulfur and nitrogen dual-doped mesoporous graphene electrocatalyst for oxygen reduction with synergistically enhanced performance. *Angew. Chem., Int. Ed.* **51**, 11496–11500 (2012).
29 Wan, C., Regmi, Y. N. & Leonard, B. M. Multiple phases of molybdenum carbide as electrocatalysts for the hydrogen evolution reaction. *Angew. Chem. Int. Ed.* **53**, 6407–6410 (2014).
30 Zheng, Y., Jiao, Y., Jaroniec, M. & Qiao, S. Z. Advancing the electrochemistry of the hydrogen-evolution reaction through combining experiment and theory. *Angew. Chem. Int. Ed.* **54**, 52–65 (2015).
31 Wang, J., Cui, W., Liu, Q., Xin, Z., Asiri, A. M. & Sun, X. Recent progress in cobalt-based heterogeneous catalysts for electrochemical water splitting. *Adv. Mater.* **28**, 215–230 (2016).
32 Deng, J., Ren, P., Deng, D. & Bao, X. Enhanced electron penetration through an ultrathin graphene layer for highly efficient catalysis of the hydrogen evolution reaction. *Angew. Chem. Int. Ed.* **54**, 2100–2104 (2015).
33 Jiang, P., Liu, Q., Liang, Y., Tian, J., Asiri, A. M. & Sun, X. A cost-effective 3D hydrogen evolution cathode with high catalytic activity: FeP nanowire array as the active phase. *Angew. Chem., Int. Ed.* **53**, 12855–12859 (2014).
34 Cao, B., Veith, G. M., Neuefeind, J. C., Adzic, R. R. & Khalifah, P. G. Mixed close-packed cobalt molybdenum nitrides as non-noble metal electrocatalysts for the hydrogen evolution reaction. *J. Am. Chem. Soc.* **135**, 19186–19192 (2013).

35 Zheng, Y., Jiao, Y., Li, L. H., Xing, T., Chen, Y., Jaroniec, M. & Qiao, S. Z. Toward design of synergistically active carbon-based catalysts for electrocatalytic hydrogen evolution. *ACS Nano.* **8**, 5290–5296 (2014).
36 Xing, Z., Liu, Q., Asiri, A. M. & Sun, X. Closely interconnected network of molybdenum phosphide nanoparticles: a highly efficient electrocatalyst for generating hydrogen from water. *Adv. Mater.* **26**, 5702–5707 (2014).
37 Cui, W. e. i., Cheng, N., Liu, Q., Ge, C., Asiri, A. M. & Sun, X. Mo_2C nanoparticles decorated graphitic carbon sheets: biopolymer-derived solid-state synthesis and application as an efficient electrocatalyst for hydrogen generation. *ACS Catal.* **4**, 2658–2661 (2014).
38 Cui, W., Liu, Q., Xing, Z., Asiri, M., Alamry, K. A. & Sun, X. MoP nanosheets supported on biomass-derived carbon flake: One-step facile preparation and application as a novel high-active electrocatalyst toward hydrogen evolution reaction. *Appl. Catal. B* **164**, 144–150 (2015).
39 Fan, X., Peng, Z., Ye, R., Zhou, H. & Guo, X. M_3C (M: Fe, Co, Ni) nanocrystals encased in graphene nanoribbons: an active and stable bifunctional electrocatalyst for oxygen reduction and hydrogen evolution reactions. *ACS Nano* **9**, 7407–7418 (2015).
40 Liao, L., Zhu, J., Bian, X., Zhu, L., Scanlon, M. D., Girault, H. H., Liu, B. MoS_2 formed on mesoporous graphene as a highly active catalyst for hydrogen evolution. *Adv. Funct. Mater.* **23**, 5326–5333 (2013).

Supplementary Information accompanies the paper on the NPG Asia Materials website (http://www.nature.com/am)